frontiers | Frontiers in Photonics

TYPE Original Research
PUBLISHED 12 April 2023
DOI 10.3389/fphot.2023.1169988

OPEN ACCESS

EDITED BY
Cheng Wang,
ShanghaiTech University, China

REVIEWED BY
Jianan Duan,
Harbin Institute of Technology, Shenzhen, China
Song-Sui Li,
Southwest Jiaotong University, China

*CORRESPONDENCE
Kathy Lüdge,
kathy.luedge@tu-ilmenau.de

SPECIALTY SECTION
This article was submitted to Non-linear Optics, a section of the journal Frontiers in Photonics

RECEIVED 20 February 2023
ACCEPTED 22 March 2023
PUBLISHED 12 April 2023

CITATION
Roos A, Meinecke S and Lüdge K (2023), Spontaneous emission noise resilience of coupled nanolasers.
Front. Photonics 4:1169988.
doi: 10.3389/fphot.2023.1169988

Spontaneous emission noise resilience of coupled nanolasers

Aycke Roos[1], Stefan Meinecke[1] and Kathy Lüdge[2]*

[1]Institut für Theoretische Physik, Technische Universität Berlin, Berlin, Germany, [2]Institut für Physik, Technische Universität Ilmenau, Ilmenau, Germany

We investigate the spontaneous emission noise resilience of the phase-locked operation of two delay-coupled nanolasers. The system is modeled by semi-classical Maxwell–Bloch rate equations with stochastic Langevin-type noise sources. Our results reveal that a polarization dephasing time of two to three times the cavity photon lifetime maximizes the system's ability to remain phase-locked in the presence of noise-induced perturbations. The Langevin noise term is caused by spontaneous emission processes which change both the intensity auto-correlation properties of the solitary lasers and the coupled system. In an experimental setup, these quantities are measurable and can be directly compared to our numerical data. The strong parameter dependence of the noise tolerance that we find may show possible routes for the design of robust on-chip integrated networks of nanolasers.

KEYWORDS

laser dynamics, coupled lasers, class-C lasers, noise resilience, unlocking transition, non-linear dynamics

1 Introduction

Over the recent years, coupled nanophotonic laser networks have found a variety of applications, e.g., in photonic integrated circuits, on-chip optical computing, and optical communication (Heil et al., 2001; Zapf et al., 2017; Ma and Oulton, 2019; Ning, 2019; Lingnau et al., 2020; Robertson et al., 2020). A wide bandwidth of new and strongly varying implementations has led to great advantages, such as a small footprint, high speed, and room temperature compatibility (Zhang et al., 2014; Deka et al., 2020). However, new challenges to the theoretical treatment of such systems have arisen from these developments. The small size of nanolasers pushes their dynamical timescales into regimes for which a description *via* conventional semiconductor laser models [class-B laser models (Arecchi et al., 1984; Erneux and Glorieux, 2010)] is no longer sufficient (van Tartwijk and Agrawal, 1998; Lingnau et al., 2019). Due to device miniaturization, the cavity photon lifetime becomes comparable to the microscopic polarization lifetime. In particular, nanolasers made of metal nanocavities (Ning, 2010), metal-coated semiconductor nanolasers (Koulas-Simos et al., 2022), or 2D materials (Du et al., 2020) exhibit high photon losses and, therefore, have shortened cavity photon lifetime (Neogi et al., 2002; Li and Ning, 2012; Zhang et al., 2014). As a consequence, the dynamic degree of freedom of microscopic polarization is important for the theoretical description in addition to the electric field and charge carrier dynamics (Lorke et al., 2013; Aust et al., 2016).

We use a Maxwell–Bloch-type laser model to describe the three aforementioned dynamical quantities in the coupled setup of two nanolasers [two delay-coupled class-C laser models (Haken, 1975; Haken, 1985; van Tartwijk and Agrawal, 1998; Ohtsubo, 2008)]. The dynamical behavior of such lasers has been investigated previously in various setups, e.g., in feedback and coupling settings (Lingnau et al., 2019; Roos et al., 2021; Wang et al.,

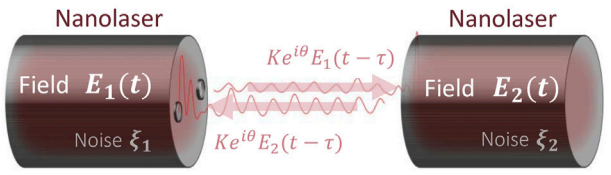

FIGURE 1
Sketch of the two coupled nanolasers described by the Maxwell–Bloch class-C equations given in Eq. 1. The solitary frequencies of the lasers are detuned by $2\delta\omega = \omega_2 - \omega_1$.

2021), and in direct comparison with class-B lasers (Hohl et al., 1997; Javaloyes et al., 2003; Erzgräber et al., 2006; Bonatto et al., 2012; Junges and Gallas, 2015; Seifikar et al., 2018). Here, we focus on the effect of spontaneous emission noise and derive insights about optimal conditions for the noise-resilient phase-locked operation of the two delay-coupled lasers. For our purpose, the exact noise distribution, e.g., as can be obtained *via* a stochastic simulator approach (Puccioni and Lippi, 2015; Wang et al., 2021), is less important. Hence, we use a simplified Langevin stochastic noise source. To quantify whether the lasers are phase-locked, we compute the phase correlation. By performing multiple parameter studies, we aim to unravel how the polarization timescale influences the noise resilience of synchronized laser emission. On that account, we limit our investigation to parameter settings that permit deterministic (i.e., without the stochastic noise source) phase locking among the two lasers. We quantify the tolerance to noise in parameter space by defining a critical noise strength which we can directly translate into the experimentally accessible intensity auto-correlation ($g^{(2)}$ function) of one laser.

2 Materials and methods

2.1 Coupled nanolaser model

The delay-coupled nanolasers are shown in Figure 1 and are described by the following set of macroscopic Maxwell–Bloch equations [class-C laser model, also used in (Roos et al., 2021)]:

$$\dot{E}_j = cP_j - \frac{E_j}{2} + (-1)^j i\delta\omega E_j + Ke^{i\theta}E_k(t-\tau) + \sqrt{\beta}\xi_j, \tag{1a}$$

$$\dot{P}_j = \frac{(i\Delta\omega - 1)P_j + E_j N_j}{T_2} + (-1)^j i\delta\omega P_j, \tag{1b}$$

$$\dot{N}_j = \frac{1}{T}\left[p - N_j - 2c\mathrm{Re}\left(P_j E_j^*\right)\right]. \tag{1c}$$

Here, the indices $j, k \in \{1, 2\}$ enumerate the two lasers. The equations describe three dynamical quantities for each laser: The inversion N of a two-level system, the complex electric field amplitude E, and the microscopic polarization P. Each of these dynamical quantities is subject to internal loss processes and thus connected to a characteristic timescale on which the corresponding dynamics evolve: T is the inversion lifetime, T_2 is the polarization lifetime, and T_{ph} is the photon lifetime. The latter has been used for transforming Eq. 1 into a non-dimensionless form, e.g., all times and frequencies are given in units of T_{ph} and T_{ph}^{-1}, respectively. A typical value for T_{ph} is on the order of 1ps for nanolasers (Ding and Ning, 2013). p is the pump supplying the lasers with energy, and $\Delta\omega$ is the difference between the transition frequency of the active laser medium and the cavity mode. In our equations, the dynamical impact of $\Delta\omega$ resembles the linewidth enhancement factor α (Schunk and Petermann, 1986; Lingnau et al., 2013). For all parameter choices, the first laser threshold is at $p_{thr}^{(1)} = 0.5$ due to the scaling with $c = ((2\Delta\omega)/(T_2 + 2))^2 + 1$. The detuning between the two lasers is $2\delta\omega$, and it is implemented such that the rotating frame used for the fields is located equidistantly between the two laser frequencies (Roos et al., 2021). In addition to detuning, the lasers are modeled with identical parameters. Tuning the other parameters typically affects the laser intensity and, thereby, also the emission frequency *via* the non-zero amplitude-phase coupling. Hence, parameter changes always produce a frequency detuning, which then dominates all other effects. To the best of our knowledge, this observation is similar to experimental observations, where other parameters, e.g., the pump or the crystal temperature, are employed to match the emission frequency of multiple lasers in coupling setups. We, therefore, assume that the frequency detuning is the most relevant parameter and omit the other parameters for the sake of simplicity.

TABLE 1 Parameters used for simulations.

Symbol	Value	Symbol	Value
$\Delta\omega$	3	τ	10
T_2	1	K	0.1
T	392	ϵ	0.05
$p_{thr}^{(1)}$	0.5	p	2

The coupling setup of the lasers is characterized by three parameters: the coupling strength K [we use a value of $K = 0.1$ corresponding to an intensity reflectivity of $\approx 20\%$ (Roos et al., 2021), where effects due to back-reflected light are negligible (Schelte et al., 2019)], the coupling phase θ describing an additional phase shift between the interfering fields, and the time delay τ of the two laser fields due to the finite propagation speed of the signals [we consider a time delay of $\tau = 10$ that refers to an on-chip coupling distance of 800 μm and can experimentally be realized; see e.g., (Deka et al., 2020)]. Spontaneous emission is included *via* a stochastic Langevin term added to the field equation, given in Eq. 1a, where ξ_j denotes a delta-correlated Gaussian white noise source and β denotes the spontaneous emission strength. It should be noted that the observed auto- and cross-correlation properties of the laser intensities not only depend on the value of β but also on all other parameters due to the coupled dynamics. The parameters are given in Table 1.

2.2 Locked emission states

A solitary class-C laser operated below its second laser threshold has a stable emission state and will show only damped relaxation oscillations toward a steady-state solution after a perturbation. Above the second threshold, periodic oscillations or deterministic chaotic behavior occurs (Lingnau et al., 2019). We will operate our laser below the onset of instabilities at four times the first threshold; however, the coupling of two class-C lasers introduces additional

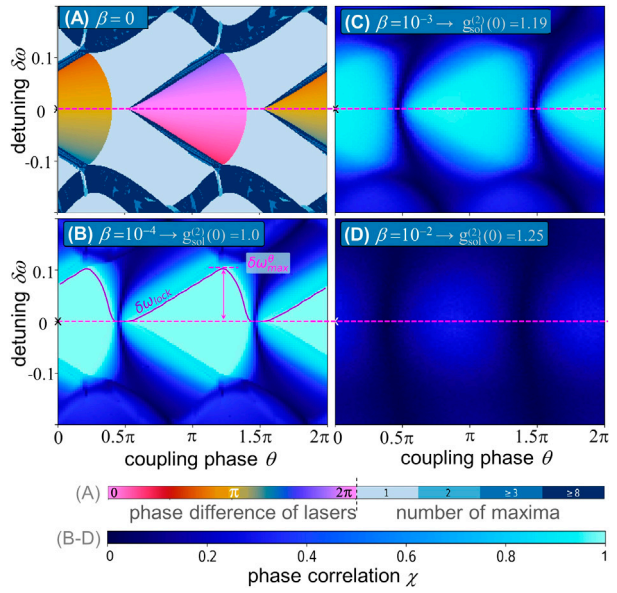

FIGURE 2
Deterministic dynamics **(A)** and phase correlation χ **(B–D)** of the two lasers in (θ, $\delta\omega$)-parameter space; **(B–D)** are obtained for noise strengths β (β and the corresponding $g^{(2)}_{sol}$ are indicated in the figure). The purple line in **(B)** shows the locking range $\delta\omega$. Parameters as given in Table 1 dashed pink line indicates 0 detuning.

emission states with complex dynamics even below the second threshold. Recently, the polarization lifetime T_2 was found to fundamentally influence the locking structure of two coupled class-C lasers (Roos et al., 2021). A scan of the dynamics found in the parameter plane of the coupling phase and the detuning is shown in Figure 2A for a dephasing time of $T_2 = 1$. The steady-state solutions, commonly referred to as compound laser modes (CLMs) (Erzgräber et al., 2006; Roos et al., 2021), can be followed in parameter space and are plotted in yellow/pink colors, as shown in Figure 2A. The color encodes the constant phase shift $\Delta\phi$ between the emission of the two lasers, $E_j(t) = \mathcal{E}_j(t)e^{i\phi_j(t)}$, which is defined as follows ($j = 1, 2$ enumerates the lasers):

$$\Delta\phi(t) = \phi_1(t) - \phi_2(t) = \text{const.} \tag{2}$$

The electric fields for laser emission on a CLM are given by a constant intensity emission of each laser with an optical frequency Ω and a constant phase shift ϕ^c_j:

$$E_j(t) = E^0_j e^{i\left(\Omega t + \phi^c_j\right)}. \tag{3}$$

In order to quantify the range for which locking is observed, the locking range $\delta\omega_{lock}$ has been introduced by Roos et al. (2021). It denotes the maximum possible detuning for which a stable CLM exists. In the deterministic case without noise (Figure 2A), the locking range is given by the extent of the yellow/pink areas in the y-direction. As can be seen in Figure 2A, the coupling phase is an important parameter for the dynamics of the system, and not every phase permits locking (there are phases where no CLM solutions exist). For our analysis, we are interested in the maximum locking range reached for the case of an optimally adjusted phase. We, therefore, define $\delta\omega^{\theta}_{\max}$, as in the study by Roos et al. (2021) *via*

$$\delta\omega^{\theta}_{\max} = \max_{\theta\in[0,2\pi)} \delta\omega_{\text{lock}}(\theta), \tag{4}$$

which then allows us to study its dependence on system timescales as, e.g., the polarization lifetime T_2. The maximum locking range is indicated in Figure 2B by the pink-dashed horizontal line.

For the stochastic case, where the Langevin noise source is applied, another measure needs to be defined to determine the transition to unlocked emission. For that, we define several tools. One quantity to identify whether the lasers remain on a CLM for a given noise strength is to look for the phase correlation of the electric fields and determine the noise strength where it overcomes a threshold (see the pink line in Figure 2B). The phase correlation χ is defined *via* the time average $\langle\cdot\rangle$,

$$\chi = |\langle e^{i\phi_1(t)}e^{-i\phi_2(t)}\rangle| = |\langle e^{i\Delta\phi(t)}\rangle|. \tag{5}$$

The phase correlation resembles the electric field correlation $\langle E_1 E_2^*\rangle = \langle \mathcal{E}_1(t)e^{i\phi_1(t)}\mathcal{E}_2(t)e^{-i\phi_2(t)}\rangle$. Since we are interested in phase synchronization among the lasers, the phase correlation is deprived of the amplitudes of the fields. If the lasers are entirely locked, the phase shift $\Delta\phi$ stays at a constant value and the phase correlation amounts to $\chi = 1$. On the other hand, if the lasers emit independently, the phase shift $e^{i\Delta\phi(t)}$ exhibits a random walk on the complex unit circle. Therefore, the correlation averages to $\chi = 0$. In general, only phase-synchronized emission states exhibit a phase correlation of $\chi = 1$, while desynchronized lasing modes exhibit a phase correlation of $\chi \neq 1$.

The intensity auto-correlation function $g^{(2)}_{jj}(0)$ of one laser within the coupled setup is defined as

$$g^{(2)}_{jj}(\Delta t) = \langle |E_j(t+\Delta t)|^2 |E_j(t)|^2\rangle / \langle |E_j(t)|^4\rangle. \tag{6}$$

It is also a good measure for describing the stochastic emission and will be used later on. It provides a value of 2 for noise-dominated emission and a value of 1 for coherent laser emission (Redlich et al., 2016).

To complete the picture and better understand the nature of the unlocking transition, we additionally consider the ensemble variance of the phase difference in order to define a diffusion coefficient D of the random walk-like dynamics of the phase (Otto et al., 2012; Redlich et al., 2017). D then also measures the state of synchronization as it is 0 for locked operation (i.e., no random walk) and larger than 0 otherwise.

$$\begin{aligned}\text{Var}\{\Delta\phi\}(t) &= \langle\Delta\phi^2(t)\rangle_{ens} - \langle\Delta\phi(t)\rangle^2_{ens} \\ &= 2D(\beta)\cdot t.\end{aligned} \tag{7}$$

The expectation value $\langle\cdot\rangle_{ens}$ is with respect to an ensemble of time series with different stochastic realizations. We find that the variance evolves linearly with time for sufficiently large times. The last equality implies that the time evolution of the variance can be modeled as an uncorrelated random walk. This only holds true for times t larger than the characteristic system timescales such that all correlations have decayed.

3 Results

Figures 2B–D show the phase correlation, as defined in Eq. 5, plotted color-coded in the two-dimensional (θ, $\delta\omega$) parameter space for three

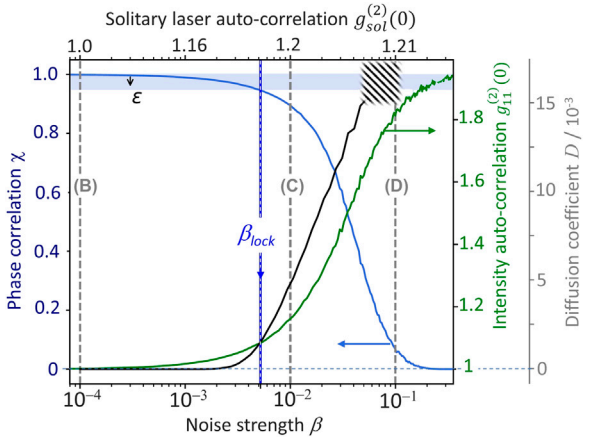

FIGURE 3
Statistical measures of the laser emission as functions of the noise strength β. The phase correlation χ is shown as a solid blue line (blue shading indicates ϵ defining the critical noise strength β_{lock}). The green and black lines show the intensity auto-correlation (Eq. 6) and the diffusion coefficient (Eq. 7). Dashed vertical lines reference panels (B–D) of Figure 2. The top x-axis indicates the auto-correlation of a solitary laser (Eq. 9). Parameters as in Table 1, $\delta\omega = 0$ and $\theta = 0$.

different noise strengths. For a noise strength of $\beta = 10^{-4}$ [see (b)], the dynamical locking structure of the deterministic system can still be seen [compare to (a)]. Here, it can be confirmed that the locked modes exhibit a phase correlation of $\chi = 1$ (light blue colors). However, if the applied noise strength β is further increased [see (c) and (d)], the phase correlation strongly decreases for each parameter set. In addition to this unlocking transition that we quantify further in the following section, the noise does not induce any new features in the investigated parameter space.

To elaborate on the physical context of the unlocking process induced by the noise, we plot the phase correlation χ as a function of the noise strength β in Figure 3 (blue line) for zero detuning and zero phase ($\delta\omega = 0$, $\theta = 0$). As expected, the phase correlation transitions from 1 to 0 as β increases. The noise strengths for which the scans of Figures 2B–D are performed can be seen as vertical dashed lines. The transition of the phase correlation gives rise to a practical possibility to quantify the unlocking of the lasers. We define the critical noise strength β_{lock} in Eq. 8 as the maximum noise strength for which the phase correlation does not exceed a certain threshold of $1 - \epsilon$ (we set $\epsilon = 0.05$).

$$\beta_{lock} = \max\{\beta | \chi(\beta) > 1 - \epsilon\}. \tag{8}$$

Figure 3 also shows the intensity auto-correlation $g^{(2)}_{11}(0)$ of one of the lasers (green line) calculated from Eq. 6 where the transition from 1 to 2 can be detected. As long as $g^{(2)}_{jj}(0) < 1.1$, we are below the locking threshold.

The critical noise strength β_{lock} that we use to define the unlocking of the lasers cannot be measured and also changes with the set of equations that is used. In order to overcome this issue, we determine the intensity auto-correlation of a single laser without coupling.

$$g^{(2)}_{sol}(0) = g^{(2)}_{11}(0)(K = 0, \beta), \tag{9}$$

which can directly be measured (Koulas-Simos et al., 2022) and is thus better suited for quantifying the amount of noise in the system. Thus, we always plot both quantities, β and $g^{(2)}_{sol}(0)$, when discussing the results (see, e.g., upper x-axis in Figure 3).

The last quantity that we evaluate to characterize the transition to unlocking is the diffusion coefficient D (black line in Figure 3). It increases from a value of 0 for low noise strengths to a maximum of $D = 15 \times 10^{-3}$ for $\beta = 0.05$. It should be noted that we excluded the region of high noise strength due to convergence problems (hashed area in Figure 3). As can be seen in Figure 3, the unlocking transition seen in quantity D is closely related to the change observed in the phase correlation χ with increasing noise strength. A diffusion coefficient of zero is found when $e^{i\Delta\phi}$ is entirely locked to a certain point on the unit circle, thus leading to $\chi = 1$. Once the lasers unlock, the diffusion coefficient D increases linearly with the noise strength. This resembles a characteristic feature of a random walk.

To understand how the noise resilience of the synchronized state changes with the coupling phase θ, we plot the phase correlation (Eq. 5) as a function of θ and β in Figure 4 (blue color code). The critical noise strength β_{lock} is printed as a blue line. As defined previously, it is the contour line that satisfies $\chi = 1 - \epsilon$ and separates regions corresponding to unlocked and locked emission states. We see that the critical noise strength strongly depends on the coupling phase θ. Within the white areas, the deterministic system does not have a stable CLM solution that can be unlocked by noise (see Figure 2A). To exclude the details of the phase effects and to be able to study the maximum possible noise resilience of our laser system, we introduce the maximum critical noise strength.

$$\beta^{\theta}_{\max} = \max_{\theta \in [0, 2\pi)} \beta_{lock}(\theta). \tag{10}$$

This quantity is used to study the impact of the internal laser timescales on noise resilience as it describes the maximum noise that can be tolerated within one laser for the case where the phase is adjusted to its optimal value. As mentioned previously, the value of the noise strength is strongly model-dependent, and we rather determine the experimentally accessible intensity auto-correlation of a solitary laser at this maximum noise strength $g^{(2)}_{sol}(0)_{\beta^{\theta}_{max}}$ (see Figure 4).

One internal timescale that is specifically important for the dynamics of the nanolasers described with our class-C laser equations is the polarization lifetime T_2. We aim to determine if there is an optimal value T_2^{opt} that maximizes the noise tolerance of the coupled system and its dependence on the frequency detuning $\delta\omega$ between the two lasers. In order to determine the value, we evaluate and plot the correlation $g^{(2)}_{sol}(0)_{\beta^{\theta}_{max}}$ of the solitary laser at the maximum critical noise strength in (T_2, $\delta\omega$)-parameter space, as shown in Figure 5. The largest relevant detuning is the deterministic maximum locking range $\delta\omega^{\theta}_{\max}$ (black line) because above that line, even without noise, there is no stable locking (no stable CLM exists). We see that $g^{(2)}_{sol}(0)_{\beta^{\theta}_{max}}$ decreases with the detuning of the lasers (dark orange). The maximum locking range $\delta\omega^{\theta}_{\max}$ (black line) is maximized by a polarization lifetime of $T_2 \approx 1$ as an optimal condition between gain bandwidth and linear system stability is reached (Roos et al., 2021). The best parameter for a large noise tolerance (large $g^{(2)}_{sol}(0)_{\beta^{\theta}_{max}}$), however, seems to be found for a T_2 between 2 and 3 (see bright regions in Figure 5). For this value of the dephasing time, a strong incoherence, i.e., noisiness, is needed to evoke a desynchronization, while a much smaller noise is sufficient to bring the laser out of synchronization at $T_2 \approx 1$. The optimal noise resistance of the coupled laser system is thus predicted to be found for a polarization lifetime of $T_2^{\text{opt}} \approx 2.5$ as long as the detuning does not exceed $\delta\omega = 0.06$.

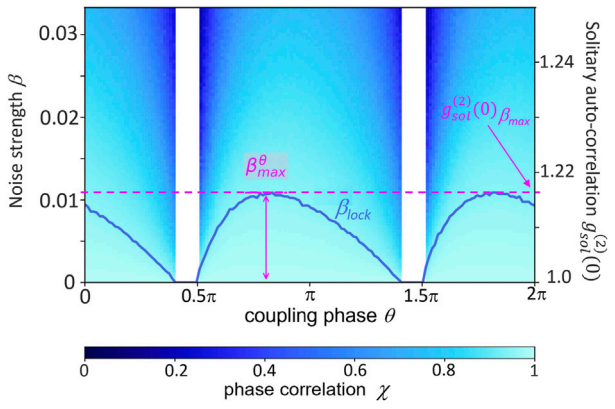

FIGURE 4
Phase correlation χ as a function of noise strength and coupling phase θ. The critical noise strength β_{lock}, as determined from Eq. 8, is shown as a blue line, and the maximum noise strength is indicated by the horizontal pink-dashed line. The right y-axis gives the intensity auto-correlation of one solitary laser. Parameters as in Table 1, $\delta\omega = 0$.

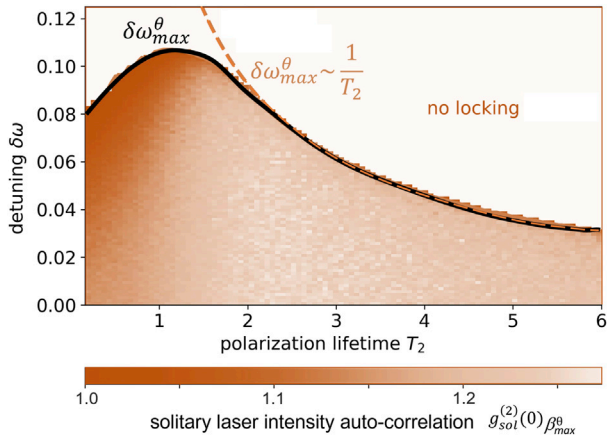

FIGURE 5
Maximum tolerated noise as a function of T_2 and detuning $\delta\omega$ color coded *via* the intensity auto-correlation $g^{(2)}_{sol}(0)_{\beta^{\theta}_{max}}$. The black line shows the maximum locking range $\delta\omega^{\theta}_{max}$, which is $\propto 1/T_2$ for large T_2. Parameters as in Table 1.

4 Conclusion

We investigated the impact of spontaneous emission noise on delay-coupled prototypical micro/nanolasers, which we describe using a Maxwell–Bloch type class-C laser model. This approach, despite its simplifications regarding the gain medium, provides valuable qualitative insights. In particular, it unravels the interplay among the different dynamical quantities and thereby highlights relevant trends. In order to quantify the noise-induced unlocking of the lasers, we have discussed the maximum tolerated noise strength in parameter space. The results for the noise strength are converted to the intensity auto-correlation of a single laser on the verge of unlocking. This enables easy comparison with experiments and other laser models. Our results revealed that the noise resilience of coupled lasers is, for small detunings, optimized by a polarization lifetime of two to three times the photon lifetime. Comparing the results for spontaneous emission noise with the behavior of the system under frequency detunings reveals an interesting trend: the lasers show a fundamentally different response to the two perturbations. The detuning locking range is maximized by a polarization lifetime of the order of the photon lifetime, which, however, leads to a drastic decrease in the noise resilience of the lasers.

Data availability statement

The raw data supporting the conclusion of this article will be made available by the authors, without undue reservation.

Author contributions

The project was initiated and lead by SM and KL. Numerical simulations were performed by AR. All authors discussed the results and wrote the manuscript.

Funding

The work was funded by the German Research Foundation within SFB910 project B9.

Conflict of interest

The authors declare that the research was conducted in the absence of any commercial or financial relationships that could be construed as a potential conflict of interest.

Publisher's note

All claims expressed in this article are solely those of the authors and do not necessarily represent those of their affiliated organizations, or those of the publisher, the editors, and the reviewers. Any product that may be evaluated in this article, or claim that may be made by its manufacturer, is not guaranteed or endorsed by the publisher.

References

Arecchi, F. T., Lippi, G. L., Puccioni, G. P., and Tredicce, J. R. (1984). Deterministic chaos in laser with injected signal. *Opt. Commun.* 51, 308–314. doi:10.1016/0030-4018(84)90016-6

Aust, R., Kaul, T., Ning, C. Z., Lingnau, B., and Lüdge, K. (2016). Modulation response of nanolasers: What rate equation approaches miss. *Opt. Quantum Electron.* 48, 109. doi:10.1007/s11082-016-0378-4

Bonatto, C., Kelleher, B., Huyet, G., and Hegarty, S. P. (2012). Transition from unidirectional to delayed bidirectional coupling in optically coupled semiconductor lasers. *Phys. Rev. E* 85, 026205. doi:10.1103/physreve.85.026205

Deka, S. S., Jiang, S., Pan, S. H., and Fainman, Y. (2020). Nanolaser arrays: Toward application-driven dense integration. *Nanophotonics* 10, 149–169. doi:10.1515/nanoph-2020-0372

Ding, K., and Ning, C. Z. (2013). Fabrication challenges of electrical injection metallic cavity semiconductor nanolasers. *Semicond. Sci. Technol.* 28, 124002. doi:10.1088/0268-1242/28/12/124002

Du, W., Li, C., Sun, J., Xu, H., Yu, P., Ren, A., et al. (2020). Nanolasers based on 2d materials. *Laser Photonics Rev.* 14, 2000271. doi:10.1002/lpor.202000271

Erneux, T., and Glorieux, P. (2010). *Laser dynamics*. (UK: Cambridge University Press. doi:10.1017/cbo9780511776908

Erzgräber, H., Krauskopf, B., and Lenstra, D. (2006). Compound laser modes of mutually delay-coupled lasers. *SIAM J. Appl. Dyn. Syst.* 5, 30–65. doi:10.1137/040619958

Haken, H. (1975). Analogy between higher instabilities in fluids and lasers. *Phys. Lett.* 53A, 77–78. doi:10.1016/0375-9601(75)90353-9

Haken, H. (1985). *Laser light dynamics*. vol. 1 1st edn. Netherlands: North Holland.

Heil, T., Fischer, I., Elsäßer, W., Mulet, J., and Mirasso, C. R. (2001). Chaos synchronization and spontaneous symmetry-breaking in symmetrically delay-coupled semiconductor lasers. *Phys. Rev. Lett.* 86, 795–798. doi:10.1103/physrevlett.86.795

Hohl, A., Gavrielides, A., Erneux, T., and Kovanis, V. (1997). Localized synchronization in two coupled nonidentical semiconductor lasers. *Phys. Rev. Lett.* 78, 4745–4748. doi:10.1103/physrevlett.78.4745

Javaloyes, J., Mandel, P., and Pieroux, D. (2003). Dynamical properties of lasers coupled face to face. *Phys. Rev. E* 67, 036201. doi:10.1103/physreve.67.036201

Junges, L., and Gallas, J. A. C. (2015). Stability diagrams for continuous wide-range control of two mutually delay-coupled semiconductor lasers. *New J. Phys.* 17, 053038. doi:10.1088/1367-2630/17/5/053038

Koulas-Simos, A., Buchgeister, J., Drechsler, M. L., Zhang, T., Laiho, K., Sinatkas, G., et al. (2022). Quantum fluctuations and lineshape anomaly in a high-beta silver-coated inp-based metallic nanolaser. *Laser Photonics Rev.* 2022, 2200086. doi:10.1002/lpor.202200086

Li, D. B., and Ning, C. Z. (2012). Interplay of various loss mechanisms and ultimate size limit of a surface plasmon polariton semiconductor nanolaser. *Opt. Express* 20, 16348. doi:10.1364/oe.20.016348

Lingnau, B., Lüdge, K., Schöll, E., and Chow, W. W. (2013). Microscopic versus α-factor descriptions of dynamics in quantum-dot lasers. *Photonics Conf. (IPC) IEEE* 22, 81–82. doi:10.1109/ipcon.2013.6656379

Lingnau, B., Perrott, A. H., Dernaika, M., Caro, L., Peters, F. H., and Kelleher, B. (2020). Dynamics of on-chip asymmetrically coupled semiconductor lasers. *Opt. Lett.* 45, 2223–2226. doi:10.1364/ol.390401

Lingnau, B., Turnwald, J., and Lüdge, K. (2019). Class-C semiconductor lasers with time-delayed optical feedback. *Phil. Trans. R. Soc. A* 377, 20180124. doi:10.1098/rsta.2018.0124

Lorke, M., Suhr, T., Gregersen, N., and Mørk, J. (2013). Theory of nanolaser devices: Rate equation analysis versus microscopic theory. *Phys. Rev. B* 87, 205310. doi:10.1103/physrevb.87.205310

Ma, R. M., and Oulton, R. (2019). Applications of nanolasers. *Nat. Nanotechnol.* 14, 12–22. doi:10.1038/s41565-018-0320-y

Neogi, A., Lee, C. W., Everitt, H. O., Kuroda, T., Tackeuchi, A., and Yablonovitch, E. (2002). Enhancement of spontaneous recombination rate in a quantum well by resonant surface plasmon coupling. *Phys. Rev. B* 66, 153305. doi:10.1103/physrevb.66.153305

Ning, C. Z. (2010). Semiconductor nanolasers. *Phys. Status Solidi B* 247, 774–788. doi:10.1002/pssb.200945436

Ning, C. Z. (2019). Semiconductor nanolasers and the size-energyefficiency challenge: A review. *Adv. Phot.* 1, 1. doi:10.1117/1.ap.1.1.014002

Ohtsubo, J. (2008). *Semiconductor lasers: Stability, instability and chaos*. 2 edn. Berlin Heidelberg: Springer-Verlag.

Otto, C., Lüdge, K., Vladimirov, A. G., Wolfrum, M., and Schöll, E. (2012). Delay-induced dynamics and jitter reduction of passively mode-locked semiconductor lasers subject to optical feedback. *New J. Phys.* 14, 113033. doi:10.1088/1367-2630/14/11/113033

Puccioni, G. P., and Lippi, G. L. (2015). Stochastic simulator for modeling the transition to lasing. *Opt. Express* 23, 2369–2374. doi:10.1364/oe.23.002369

Redlich, C., Lingnau, B., Holzinger, S., Schlottmann, E., Kreinberg, S., Schneider, C., et al. (2016). Mode-switching induced super-thermal bunching in quantum-dot microlasers. *New J. Phys.* 18, 063011. doi:10.1088/1367-2630/18/6/063011

Redlich, C., Lingnau, B., Huang, H., Raghunathan, R., Schires, K., Poole, P. J., et al. (2017). Linewidth rebroadening in quantum dot semiconductor lasers. *IEEE J. Sel. Top. Quantum Electron.* 23, 1–10. doi:10.1109/jstqe.2017.2701555

Robertson, J., Hejda, M., Bueno, J., and Hurtado, A. (2020). Ultrafast optical integration and pattern classification for neuromorphic photonics based on spiking vcsel neurons. *Sci. Rep.* 10, 6098. doi:10.1038/s41598-020-62945-5

Roos, A., Meinecke, S., and Lüdge, K. (2021). Stabilizing nanolasers via polarization lifetime tuning. *Sci. Rep.* 11, 18558. doi:10.1038/s41598-021-97757-8

Schelte, C., Camelin, P., Marconi, M., Garnache, A., Huyet, G., Beaudoin, G., et al. (2019). Third order dispersion in time-delayed systems. *Phys. Rev. Lett.* 123, 043902. doi:10.1103/physrevlett.123.043902

Schunk, N., and Petermann, K. (1986). Noise analysis of injection-locked semiconductor injection lasers. *IEEE J. Quantum Electron.* 22, 642–650. doi:10.1109/jqe.1986.1073018

Seifikar, M., Amann, A., and Peters, F. H. (2018). Dynamics of two identical mutually delay-coupled semiconductor lasers in photonic integrated circuits. *Appl. Opt.* 57, E37–E44. doi:10.1364/ao.57.000e37

van Tartwijk, G. H. M., and Agrawal, G. P. (1998). Laser instabilities: A modern perspective. *Prog. Quantum Electron.* 22, 43–122. doi:10.1016/s0079-6727(98)00008-1

Wang, T., Jiang, C., Zou, J., Yang, J., Xu, K., Jin, C., et al. (2021). Nanolasers with feedback as low-coherence illumination sources for speckle-free imaging: A numerical analysis of the superthermal emission regime. *Nanomaterials* 11, 3325. doi:10.3390/nano11123325

Zapf, M., Röder, R., Winkler, K., Kaden, L., Greil, J., Wille, M., et al. (2017). Dynamical tuning of nanowire lasing spectra. *Nano Lett.* 17, 6637–6643. doi:10.1021/acs.nanolett.7b02589

Zhang, Q., Li, G., Liu, X., Liu, Y., Sum, T. C., Lieber, C. M., et al. (2014). A room temperature low-threshold ultraviolet plasmonic nanolaser. *Nat. Commun.* 5, 4953. doi:10.1038/ncomms5953